machines

MDPI

Article

Vibration Isolation and Trajectory Following Control of a Cable Suspended Stewart Platform

Xuechao Duan [1,2,*], Jianwei Mi [1] and Ze Zhao [1]

[1] Key Laboratory of Electronic Equipment Structure Design, Ministry of Education of China, Xidian University, Xi'an 710071, China; jackiemi@126.com (J.M.); xazhaoze@163.com (Z.Z.)

[2] Collaborative Innovation Center of Information Sensing and Understanding, Xidian University, Xi'an 710071, China

* Correspondence: xchduan@xidian.edu.cn; Tel.: +86-29-8820-3040

Academic Editor: Dan Zhang

Received: 22 May 2016; Accepted: 18 October 2016; Published: 25 October 2016

Abstract: To achieve high-quality vibration isolation and trajectory following control of a cable driven parallel robot based Stewart platform in the five hundred meter aperture spherical radio telescope (FAST) design, the integrated dynamic model of the Stewart platform including the electric cylinder is established in this paper, the globally feedback linearization of the dynamic model is implemented based on the control law partitioning approach. To overcome the disadvantages of the external disturbance on the base and unmodeled flexibility of the mechanism, a PID (Proportional-Derivative-Integral) controller with base acceleration feedforward is designed in the operational space of the Stewart platform. Experiments of the vibration isolation and trajectory following control of the cable suspended Stewart platform with presence of the base disturbance is carried out. The experimental results show that the presented control scheme has the advantage of stable dynamics, high accuracy and strong robustness.

Keywords: FAST; Stewart platform; feedback linearization; acceleration feedforward; dynamics and control

1. Introduction

As a favourable solution to the Square Kilometre Array (SKA) plan for astronomy, China's five-hundred-meter aperture spherical radio telescope (FAST) has attracted global attention since its conceptual advent. This ongoing national major infrastructure for science is currently being constructed in the unique karst limestone formation in the southwest China and will be completed in 2017 [1–3]. Once put into operation in the near future, it will be the largest single dish super antenna in the world. It is therefore endowed the obligation to discover new stars and extraterrestrial intelligence. As a highlight of structural design, the cable supporting subsystem for the feed (radio waves receiver), which integrates mechanical, electronic and optical technologies, effectively reduces the weight and cost of the supporting structure (see Figure 1).

As shown in Figure 1, the six steel cables driven by servo motors and winches are the limbs of the first level cable-driven parallel manipulator (CDPM), with the semi-spherical feed cabin as the end-effector [4,5]. The second level subsystem of Stewart platform is mounted on the bottom of the cabin. The trajectory for the feed when observing a radio target will be as large as a circle with the radius of 186 m and height of 150 m, but real-time RMS (Root Mean Squred) of positioning and orientating error for the feed must be less than 4 mm and 8 arc-minute, respectively [6]. Consequently, the goal of this CDPM based Stewart platform is to provide both large manipulating workspace and high accuracy of the feed.

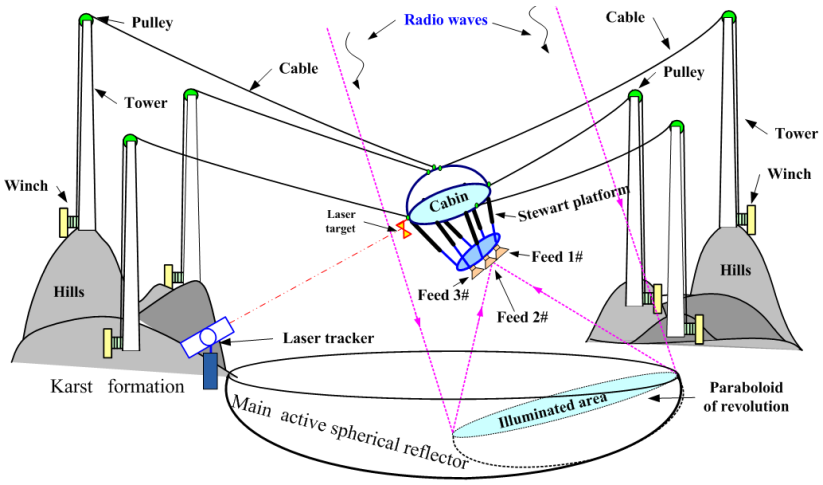

Figure 1. Overview schematic of the supporting structure for five-hundred-meter aperture spherical radio telescope (FAST).

As one of the most celebrated parallel manipulators, the Stewart platform (see Figure 2) has found wide applications in motion generating, docking of space crafts, surgical operation and numerically controlled machining since it was proposed in the 1960s [7–10]. The CDPM based fine tuning Stewart platform in this research broadens the area of its application. From the system point of view, the performance of a robotic manipulator depends not only the structural design, but also the control scheme and implementation. The Stewart platform is a complicated multiple-input multiple-output nonlinear system, and its dynamics are thus characterized by time variant, strong coupling and nonlinearity. Thus, the dynamics and control of Stewart platform is still a challenging problem in the field of robotics [10–15]. In general, the control pattern of a parallel manipulator can be divided into two categories: joint space control and workspace control [10,12]. The joint space control is a conventional single-input single-output control pattern and is actually a trajectory tracking control of following the desired joint trajectory computed from the position command of the end-effector by inverse kinematics. Therefore, most controllers in applications are based on the joint space coordinates, due to the fact that only an approximated joint model is enough for this control pattern [11–13]. On the contrary, the workspace control implies that the control is designed based on the dynamics described in the workspace coordinates. However, the controller design in workspace coordinates needs information of a 6-DOF (degree of freedom) sensor to measure the displacement or velocity of the mobile plate. Hence, the workspace control for parallel manipulator is seldom used in practice [8,10,15].

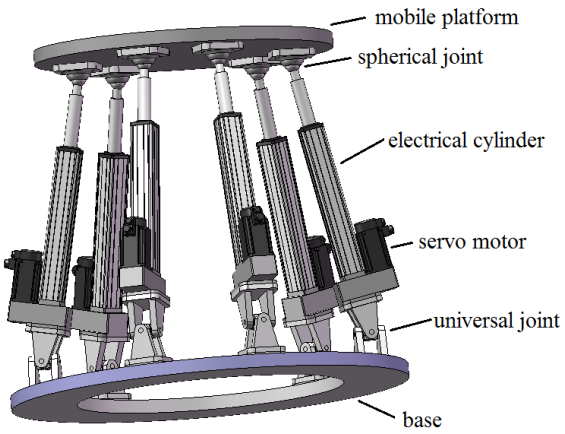

Figure 2. Schematic diagram of the Stewart platform.

Since the mobile platform of Stewart platform is driven by the six electric cylinders in parallel, there exists considerable dynamic coupling among the six electric cylinders. In addition, there also exits dynamic coupling between the Stewart platform and its cable suspended base (bottom plate of the feed cabin). Consequently, the control of Stewart platform in this application is related more to technical challenges compared to those with fixed bases. Some literature reported the preliminary research on this issue. Zhang and Wang [16] proposed the kinematics based interpolation strategy in joint space for a flexible supported Stewart platform; by combining the position prediction according to the velocity differentiation of the flexible base, they accomplished the trajectory tracking control of the end-effector. Cheng and Ren [17] established the dynamic model of the flexible supported Stewart platform via multibody system dynamics approach for simulation; however, the control action for the legs was still exerted in terms of length rather than force. Zhou and Qi [18] presented a velocity control solution for the flexible supported Stewart platform in a double-level positioning system and validated the satisfactory precision of their solution by experiments.

From the system point of view, the multiple-input multiple-output controller based on a dynamic model will be able to provide better performance than the single-input single-output controller designed in joint space for each leg instead of considering the dynamics of the platform [11,13]. On the other hand, the positioning and orientating precision of the Stewart platform with the kinematics model based control depends on the precision of the electric cylinders. In order to optimize the dynamical performance and improve the precision of the Stewart platform, it is desirable to carry out tentative research on the dynamic model based control scheme in workspace [11–14].

In this paper, the entire dynamics of the Stewart platform including the dynamics of the mechanism and property of the electric cylinder is established firstly. Then, the globally feedback linearization of the dynamic model is implemented by employing the control law partitioning approach. To overcome the disadvantages of the external disturbance on the base and unmodeled flexibility of the mechanism, a PID (Proportional-Derivative-Integral) controller with base acceleration feedforward is designed in the workspace of the Stewart platform. Field experiments were also carried out on the 1/10 scaled model.

We begin this paper with an introduction of the application of Stewart platform in the super radio telescope. In Section 2, the closed-form dynamics of Stewart platform is elaborated. The PID control law with acceleration feedforward of the base for the Stewart platform is developed in Section 3 and the 1/10 scaled model of FAST is described in Section 4. In Section 5, two representative experiments and discussion are dealt with. Finally, some meaningful conclusions and future work are presented in Section 6.

2. Closed-Form Entire Dynamics of Stewart Platform

2.1. Equation of Driving Force for an Electric Cylinder Leg

As shown in Figure 3a, an electric cylinder (a.k.a electrical linear actuator) is a mechatronic actuator consisting of a DC blushless servo motor, lead screw and related transmission components. It is used to provide linear motion or force in all types of applications. In this research, a synchronized conveying belt is employed to transmit the rotation of the servo motor to the lead screw. Since the belt is flexible by its nature, the frames and bearings of the servo motors also have finite stiffness and flexibility [19–21]. Therefore, mechanical deformation occurs in the driving axis and components under the load. For the systems with high acceleration and precision specifications, the effect of the elastic deformation on the system performance is no longer negligible. Taking the elastic deformation of the conveying belt for an example, it will introduce an energy-storing property when transmitting high-speed motion. Under the circumstance of low damping, it probably leads to high-order mechanical resonance in the transmission. Mechanical resonance of a mechatronic system will necessarily deteriorate its stability and dynamical performance [21–23].

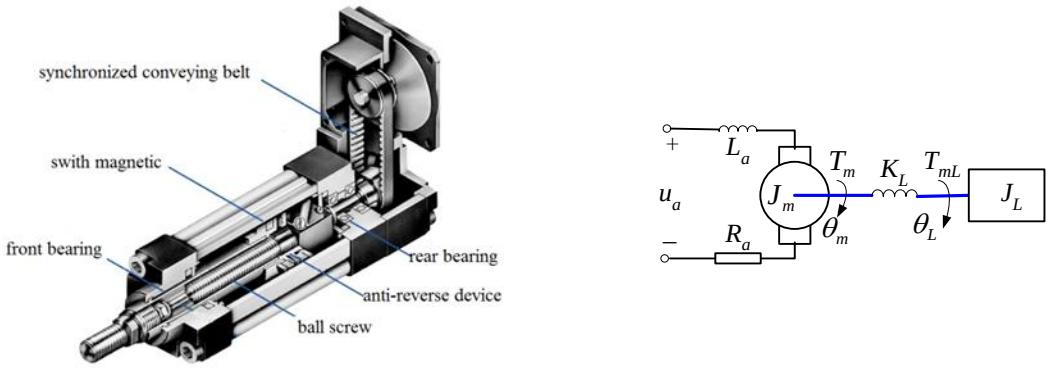

(**a**) (**b**)

Figure 3. Schematic diagram of the Stewart platform. (**a**) Mechanical schematic of the electric cylinder; and (**b**) equivalent diagram of the electric cylinder.

For the reasons mentioned above, in order to get better knowledge of the dynamical system, the electric cylinder is considered as a two-mass system consisting of a servo motor, load and equivalent transmission components between them. As shown in Figure 3b, T_m is the electromagnetic torque from the motor shaft. T_{mL} is the output torque from the ball screw; F_{mL} is the output driving force of the electric cylinder; θ_m and θ_L are angular displacement of the servo motor and nut of the ball screw. Other mechanical and electrical parameters are listed in Table 1, and we can further derive the block diagram shown in Figure 4 and the transfer function in Equation (1) of the electric cylinder under the condition that the input is the driving voltage and the output is the driving force:

$$G(s) = \frac{F_{mL}(s)}{U_a(s)} = \frac{K_m K_L K_{FT}(J_L s + b_L)}{a_4 s^4 + a_3 s^3 + a_2 s^2 + a_1 s + a_0}, \quad (1)$$

where,

$$a_4 = J_m J_L L_a;$$
$$a_3 = L_a (J_L b_m + J_m b_L) + (R_a + K_i) J_m J_L;$$
$$a_2 = (R_a + K_i)(J_L b_m + J_m b_L) + (J_m K_L + b_m b_L) L_a + (L_a K_L + K_m C_e) J_L;$$
$$a_1 = (R_a + K_i)(K_L J_L + J_m K_L + b_m b_L) + (b_m + b_L) L_a K_L + K_m C_e b_L;$$
$$a_0 = K_m C_e K_L + (K_i + R_a)(b_m + b_L) K_L.$$

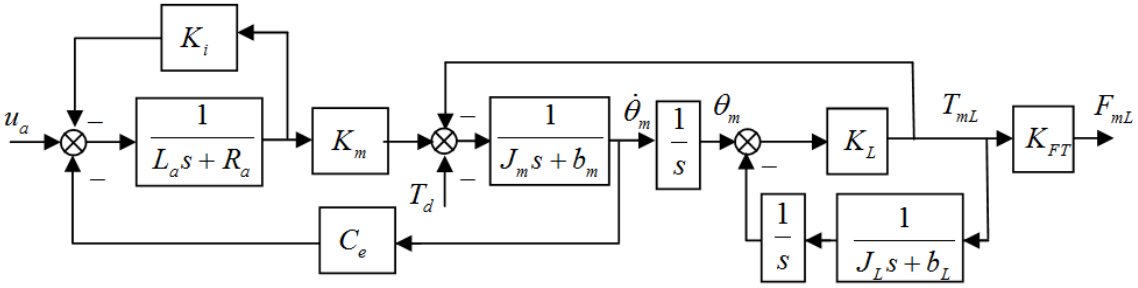

Figure 4. Block diagram of the electric cylinder in the Stewart platform.

Table 1. Specification parameters of the electric cylinder.

Symbol	Physical Sense	Value and Unit
J_m	moment of inertia of the servo motor shaft	2.2×10^{-5} kg·m^2
J_L	equivalent moment of inertia of load on ball screw	2.4×10^{-5} kg·m^2
b_m	viscous damping coefficient of the motor shaft	2.5×10^{-3} N·s/rad
K_L	Equivalent stiffness of the belt and motor shaft	293.36 Nm/rad
b_L	viscous damping coefficient of the ball screw	3.0×10^{-3} N·s/m
K_i	current feedback coefficient of the motor armature	0.02
R_a	resistance of the motor armature	0.4 Ω
L_a	inductance of the motor armature	0.0173 H
C_e	Coefficient of counter electromotive force	5.0×10^{-3} V·min/rev
K_m	Coefficient of electromagnetic force	0.85 Nm/A
K_{FT}	Coefficient of transmission of torque to thrust	1256.6

Substitution of parameters in Table 1 into Equation (1) yields the transfer function of the electric cylinder as follows:

$$G(s) = \frac{6.67s + 826.64}{9.21 \times 10^{-12}s^4 + 2.41 \times 10^{-9}s^3 + 2.42 \times 10^{-4}s^2 + 0.0346s + 104.00}.$$

Therefore, the nominal transfer function of the electric cylinder is

$$G(s) = \frac{F_{mL}(s)}{U_a(s)} \approx 0.06(s + 123.93), \tag{2}$$

where $F_{mL}(s)$ and $U_a(s)$ are Laplace transformation functions of input and output of the electric cylinder, respectively. From Equation (2), one can observe that the nominal model of the electric cylinder displays a first-order differential property due to its friction and elastic effect being stronger than its inertial effect. This phenomenon is a distinction between traditional modeling of a general DC servo motor [22,23]. Moreover, the approximation-induced variation between the nominal and physical models is considered as model perturbation [19,21], which will be tackled in the following design of the control algorithm.

2.2. Dynamics of the Stewart Platform

In this research, the legs of the Stewart platform are connected to the base with universal joints and connected to the mobile platform with spherical joints. The change of the leg lengths controls the position and orientation of the mobile platform. The base frame denoted by $OXYZ$ as shown in Figure 5 is developed, with the origin at the center of the base. The mobile feed platform frame denoted by $pxyz$ is fixed on the mobile platform, with the origin at the center of the mobile platform. The local frame $U_i x_i y_i z_i$ ($i = 1, 2, \ldots, 6$) is attached to the upper part of each leg with its origin at the rotation center of the universal joint, x_i-axis along the leg, y_i-axis along the rotating axis (axis fixed to the leg) of the universal joint and z_i-axis perpendicular to the x_i and y_i axes according to the right hand rule. Another frame $D_i x_i y_i z_i$ ($i = 1, 2, \ldots, 6$) with the same orientation for the same value of i, is attached to the lower part of the leg with the origin at the at the rotation center of the spherical joint.

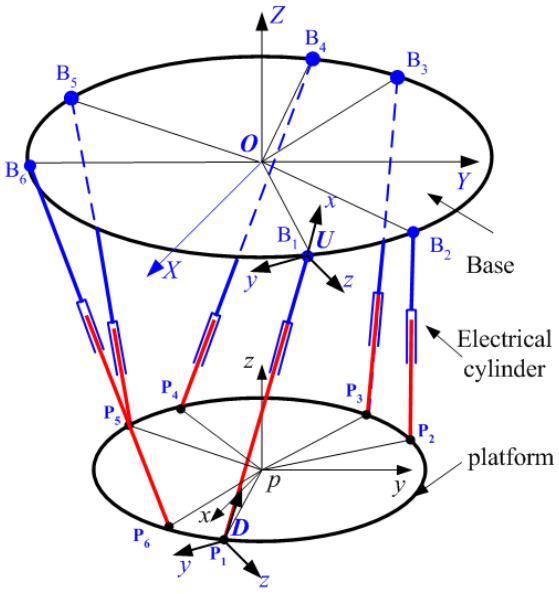

Figure 5. Schematic diagram of Stewart platform.

Let $\boldsymbol{b_i}$ be the i-th base joint point vector of B_i in the base frame, and $\boldsymbol{p_i}$ be the platform joint point vector of P_i in $pxyz$. $\boldsymbol{p} = (x, y, z)^{\mathrm{T}}$ represents the position vector of the origin p of the mobile frame $pxyz$ referred to $OXYZ$. The orientation of the mobile platform is described with the fixed angles convention, and $\Delta = (\phi, \theta, \psi)^{\mathrm{T}}$ indicates the angular rotation vector to the X, Y, Z axes of $OXYZ$, separately. Then, the i-th leg vector in the base frame can be expressed as

$$\boldsymbol{l}_i = \boldsymbol{p} + \boldsymbol{q}_i - \boldsymbol{b}_i, \tag{3}$$

where $\boldsymbol{q}_i = \Re\overline{\boldsymbol{p}}_i$ and $\Re$ is the rotation matrix of frame $pxyz$ relative to $OXYZ$ [19,22].

Therefore, once given the position and orientation of the mobile platform referred to the base, the corresponding length of the i-th leg can be calculated and the velocity of the platform-connection-point of the i-th leg is

$$\dot{\boldsymbol{l}}_i = \omega \times \dot{\boldsymbol{q}}_i + \dot{\boldsymbol{p}}, \tag{4}$$

where ω is the angular velocity of the mobile platform. The sliding velocity between the two parts of the i-th leg is given by the component of this velocity in the i-th leg direction

$$\dot{l}_i = \boldsymbol{u}_i \cdot \dot{\boldsymbol{l}}_i, \tag{5}$$

where $\boldsymbol{u}_i = \boldsymbol{l}_i / ||\boldsymbol{l}_i||$ is the unit vector of the i-th leg. The acceleration of the platform-connection-point is the time derivative of the velocity and is expressed in terms of the linear and angular acceleration of the platform as

$$\ddot{\boldsymbol{l}}_i = \varepsilon \times \boldsymbol{q}_i + \omega \times (\omega \times \boldsymbol{q}_i) + \ddot{\boldsymbol{p}}, \tag{6}$$

where $\boldsymbol{\varepsilon}$ is the angular acceleration of the mobile platform. $\ddot{\boldsymbol{l}}_i$ can be expressed in terms of the sliding acceleration $\ddot{l}_i$ at the prismatic joint and the angular acceleration $\boldsymbol{a}_{li}$ of the i-th leg as

$$\ddot{\boldsymbol{l}}_i = \ddot{l}_i \boldsymbol{u}_i + \omega_{li} \times (\omega_{li} \times \boldsymbol{l}_i) + 2\omega_{li} \times \dot{\boldsymbol{l}}_i \boldsymbol{u}_i + \boldsymbol{a}_{li} \times \boldsymbol{l}_i, \tag{7}$$

where ω_{li} and $\boldsymbol{a}_{li}$ denote the angular velocity and acceleration of the i-th leg, respectively. Taking account of $\boldsymbol{u}_i \cdot \omega_{li} = 0$ and simplifying lead to

$$\ddot{l}_i = \boldsymbol{u}_i \cdot \ddot{\boldsymbol{l}}_i + \boldsymbol{l}_i \omega_{li} \cdot \omega_{li}. \tag{8}$$

Based on the Newton-Euler formulations developed by Dasgupta and Mruthyunjaya [24] and revised by Fu, Yao and Wu [25], the inverse dynamics of the Stewart platform is available with the base, mobile platform and limb electric cylinder assumed to be rigid bodies. Because of the symmetry of the mechanism, the analysis of the single limb electric cylinder can be applied to the others. By employing the Newton-Euler formulations and combining the inverse kinematic and dynamical equations of the legs and the mobile platform, the following dynamic model of the Stewart platform system can be obtained with a series of transformations and simplifications:

$$\boldsymbol{JF} = \boldsymbol{D}, \tag{9}$$

where,

$$\boldsymbol{J} = \begin{bmatrix} \mathbf{u}_1 & \mathbf{u}_2 & \mathbf{u}_3 & \mathbf{u}_4 & \mathbf{u}_5 & \mathbf{u}_6 \\ \mathbf{q}_1 \times \mathbf{u}_1 & \mathbf{q}_2 \times \mathbf{u}_2 & \mathbf{q}_3 \times \mathbf{u}_3 & \mathbf{q}_4 \times \mathbf{u}_4 & \mathbf{q}_5 \times \mathbf{u}_5 & \mathbf{q}_6 \times \mathbf{u}_6 \end{bmatrix}^{\mathrm{T}}, \tag{10}$$

$$\mathbf{F} = (F_1,\, F_2,\, F_3,\, F_4,\, F_5,\, F_6)^{\mathrm{T}},$$

$$\boldsymbol{D} = \begin{bmatrix} \Re\mathbf{F}_{ext} + M(\boldsymbol{g} - \boldsymbol{a}) - \sum_{i=1}^{6} \mathbf{K}_i \\ \Re\mathbf{r}_0 \times M(\boldsymbol{g} - \boldsymbol{a}) - \boldsymbol{I}\varepsilon - \omega \times \boldsymbol{I}\omega + \Re\mathbf{M}_{ext} - \sum_{i=1}^{6} (\Re\mathbf{p}_i \times \mathbf{K}_i) + \sum_{i=1}^{6} C_{si}(\boldsymbol{\omega}_{li} - \boldsymbol{\omega}) \end{bmatrix}. \tag{11}$$

The $\mathbf{D} \in R^{6\times1}$ in Equation (12) includes the loads and inertia forces of the platform and the legs. The $\mathbf{F} \in R^{6\times1}$ in Equation (12) represents the input force vector of the Stewart platform, and the 6×6 matrix $\boldsymbol{J}$ denotes the Jacobian matrix mapping the input and output forces. In the above equations, the subscript i represents the i-th leg, and $i = 1, 2, \ldots, 6$. $F_i = \boldsymbol{u}_i \cdot \boldsymbol{F}_{si}$ is the component of $\boldsymbol{F}_{si}$ along the i-th leg, and $\boldsymbol{F}_{si}$ is the acting force of the i-th spherical joint on the platform with the following form

$$\boldsymbol{F}_{si} = \boldsymbol{u}_i F_i + \boldsymbol{K}_i. \tag{12}$$

Then, the constraint force of the i-th universal joint is

$$\boldsymbol{F}_{ui} = m_{ui}\boldsymbol{a}_{ui} + m_{di}\boldsymbol{a}_{di} - (m_{di} + m_{ui})\boldsymbol{g} - \boldsymbol{F}_{si}, \tag{13}$$

where $\boldsymbol{F}_{ext}$ is the external force acting on the mobile platform in the local frame. M stands for the mass of the mobile platform. $\boldsymbol{g}$ is the acceleration of gravity and $\mathbf{a}$ is the linear acceleration of the mobile platform. $\boldsymbol{K}_i = (\boldsymbol{E}_i \times \boldsymbol{u}_i)/l_i, \boldsymbol{E}_i = \boldsymbol{r}_{di} \times m_{di}\boldsymbol{a}_{di} + \boldsymbol{r}_{ui} \times m_{ui}\boldsymbol{a}_{ui} - (m_{di}\boldsymbol{r}_{di} + m_{ui}\boldsymbol{r}_{ui}) \times \mathbf{g} + (\boldsymbol{I}_{di} + \boldsymbol{I}_{ui})\boldsymbol{a}_{li} + \omega_{lii} \times (\boldsymbol{I}_{di} + \boldsymbol{I}_{ui})\omega_{li} + C_{ui}\omega_{li} + C_{si}(\omega_{li} - \boldsymbol{\omega})$. The main parameters are listed in Table 2. In addition, $\boldsymbol{r}_{di}$ and $\boldsymbol{r}_{ui}$ denote the position vectors of the centers of gravity of the lower and the upper parts in the global frame, respectively. $\boldsymbol{a}_{di}$ and $\boldsymbol{a}_{ui}$ are the acceleration of the centers of gravity of the lower and the upper part of the leg. $\boldsymbol{I}_{ui}$ and $\boldsymbol{I}_{di}$ are the moments of inertia of the upper and lower part of the leg in inertial coordinates, respectively, and they can be obtained from their moments of inertia $\boldsymbol{I}_{ui0}$ and $\boldsymbol{I}_{di0}$ in their local coordinates by the rotation transformation.

Table 2. Main parameters of the Stewart platform.

Symbol	Physical Sense	Value and Unit
M	mass of the mobile platform	5.5 kg
r_0	COG of the mobile platform	$(0,0,0)^{\mathrm{T}}$
m_{di}	mass of the upper part of leg	3.5 kg
m_{ui}	mass of the lower part of leg	2.5 kg
r_{u0}	COG of the upper part of leg	$(-0.22,0,0)^{\mathrm{T}}$
r_{d0}	COG of the lower part of leg	$(0.16,0,0)^{\mathrm{T}}$
C_{ui}	viscous coefficients at the universal joint	0.001
C_{si}	viscous coefficients at the spherical joint	0.002
ω	angular velocity of the mobile platform	variable
ε	angular acceleration of the mobile platform	variable
$\boldsymbol{M}_{ext}$	external moment acting on the mobile platform in the local frame	variable

The external force and moment acting on the mobile platform are assumed to be zero for consistency with the work condition. The dynamical equations of the Stewart platform are simplified as the following Equation (15) by separating the linear and angular acceleration terms out

$$\boldsymbol{J}\boldsymbol{F} = \begin{bmatrix} M\boldsymbol{a} \\ \boldsymbol{I}\varepsilon \end{bmatrix} + \begin{bmatrix} M\boldsymbol{g} - \sum_{i=1}^{6} \mathbf{K}_i \\ \Re\mathbf{r}_0 \times M(\boldsymbol{g}-\boldsymbol{a}) - \omega \times \boldsymbol{I}\omega - \sum_{i=1}^{6} (\Re\mathbf{b}_i \times \mathbf{K}_i) + \sum_{i=1}^{6} C_{si}(\boldsymbol{\omega}_{li} - \boldsymbol{\omega}) \end{bmatrix}. \quad (14)$$

For the purpose of mechanical design of the Stewart platform, the constraint forces are of great importance. After $\boldsymbol{F}$ is known, the equations for the legs are decoupled and the forces in different legs can be determined separately. The constraint forces of the universal and spherical joints are calculated as the more detailed description in References [24,25].

For the i-th leg one can obtain from Equation (2):

$$F_{mLi} = 0.06\dot{u}_{ai} + 7.44u_{ai},\ i = 1,2,\ldots,6. \quad (15)$$

Furthermore, the relationship of the input force vector of Stewart platform and output force vector of the six electric cylinders is subject to Equation (16):

$$\boldsymbol{F} = (F_{ml1}, F_{ml2}, F_{ml3}, F_{ml4}, F_{ml5}, F_{ml6})^{\mathrm{T}}. \quad (16)$$

Thus far, Equations (14)–(16) constitute the complete dynamics of the Stewart platform.

2.3. Control Law Partition Based Globally Feedback Linearization of the Stewart Platform

Let $\mathbf{X}, \dot{\mathbf{X}} = (\nu^{\mathrm{T}}, \omega^{\mathrm{T}})^{\mathrm{T}}, \ddot{\mathbf{X}} = (\boldsymbol{a}^{\mathrm{T}}, \varepsilon^{\mathrm{T}})^{\mathrm{T}}$ be generalized displacement, velocity and acceleration, respectively. Then Equation (14) can be rewritten as

$$\boldsymbol{M}(\boldsymbol{X})\ddot{\boldsymbol{X}} + \boldsymbol{g}(\boldsymbol{X}, \dot{\boldsymbol{X}}) = \boldsymbol{J}\boldsymbol{F}, \quad (17)$$

where $\mathbf{M}(\mathbf{X})$ is the 6×6 inertia matrix of the Stewart platform, $\mathbf{g}(\mathbf{X}, \dot{\mathbf{X}})$ is the 6×1 vector including centrifugal, Coriolis and gravity terms. By applying the control law partition to the complex dynamics described in Equation (17), one can obtain the model based control law as

$$\boldsymbol{F} = \alpha\boldsymbol{F}' + \beta, \quad (18)$$

where **F** is the driving force vector of the six electric cylinders. It is assumed that

$$\begin{cases} \alpha = \mathbf{J}^{-1}\boldsymbol{M}(\boldsymbol{X}) \\ \beta = \mathbf{J}^{-1}\boldsymbol{g}(\boldsymbol{X}, \dot{\boldsymbol{X}}) \end{cases}, \tag{19}$$

where $\boldsymbol{J}^{-1}$ is the inverse of the Jacobian matrix of the Stewart platform. In terms of Equations (17)–(19), one can derive $\mathbf{F}\prime = \ddot{\mathbf{X}}$. This result shows that the dynamics of the Stewart platform can be divided into the servo control law based linear part and model based nonlinear part. The nonlinear dynamics of the Stewart platform is simplified to the second order linear system, and this operation is called the globally feedback linearization. On the basis of this linearized model, the controller design is straightforward according to feedback control theory.

3. PID Control Law with Acceleration Feedforward of the Base for the Stewart Platform

3.1. Real-Time Acceleration Estimation of the Base

From the mechanics point of view, the main difference between the CDPM based Stewart platform and that with a fixed base lies in the nonholonomic constraints of the base. As a result of the external disturbances (wind load and vibrations of cables of the CDPM) and dynamical interaction between the cabin and Stewart platform, the feed cabin often displays small-amplitude multiple degree-of-freedom vibration near its equilibrium. On the other hand, the vibrations of the feed cabin will affect the positioning and orientation of the feed platform, i.e., the end-effector of the Stewart platform. Consequently, it is of great necessity to feed forward the motion information of the cabin into the control system of the Stewart platform so that the high precision trajectory following of the feed platform can be achieved. According to Newton's Second Law, the acceleration is the straightest reflection due to its proportional relation to force applied on the object. Therefore, compared with position and velocity, the acceleration reflects straighter the knowledge of the force applied on the system. Thus, in order to suppress the dynamical interaction between the feed cabin and the Stewart platform, the acceleration is fed forward to the control algorithm in this research. However, from the hardware point of view, it is of high cost in certain cases for measuring the acceleration of an object [12,19,22], and only the position and orientation information is measured in this research with a laser tracker. In terms of these reasons, the real-time estimation of velocity and acceleration based on the position and orientation of the feed cabin is a fundamental issue in this research.

From the kinematics of mechanical system, one can infer that there exists linear differentiation relation among the position, velocity and acceleration. The differentiator algorithm is needed in common tracking and prediction strategy to obtain the velocity from position signal and acceleration from velocity signal. The problem is that the ordinary differentiator also amplifies the noise signal mixed in the measuring data. To overcome this problem, a low-pass filer often is employed. However, the filter results in phase lag when dealing with high frequency noise, which deteriorates the stability of the control system and narrows the bandwidth.

Thus, this research adopts a novel nonlinear tracking differentiator (NTD) playing an important role in the active disturbance rejection controller proposed by Han [26,27]. It achieves the goals of obtaining the differential signals from discontinuous or noisy measuring signals in engineering practice. This prediction algorithm needs to abstract the velocity and acceleration signals from the leg length signals.

The second-order tracking differentiator has the following discrete form:

$$\begin{cases} r_1(k+1) = r_1(k) + h \cdot r_2(k) \\ r_2(k+1) = r_2(k) + h \cdot fhan(r_1(k) - r(k), r_2(k), \delta, h) \end{cases}, \tag{20}$$

where h is the sampling step, and δ is the velocity factor determining the transient process. The nonlinear function $fhan(x_1, x_2, \delta, h)$ is expressed by

$$fhan(x_1, x_2, \delta, h) = \begin{cases} -\delta \cdot \mathrm{sgn}(a), & |a| > d \\ -\delta \cdot a/d, & |a| \leq d \end{cases}, \tag{21}$$

where $\mathrm{sgn}(\cdot)$ indicates the sign function, and the parameters a and d of the nonlinear function are defined as the following:

$$a = \begin{cases} x_2 + \frac{a_0 - d}{2}\mathrm{sgn}(y), & |y| > d_0 \\ x_2 + y/2, & |y| \leq d_0 \end{cases}, \tag{22}$$

$$\begin{cases} d = h\delta, d_0 = hd \\ y = x_1 + hx_2 \\ a_0 = \sqrt{d^2 + 8\delta\,|y|} \end{cases}, \tag{23}$$

where d and d_0 are switching thresholds of the function, y is the combinatorial value of the state variables, and a and a_0 are the net increment of the state variable values of the function.

For any limitary integrable function $r(t)$, the two signals $r_1(t)$ and $r_2(t)$ provided by Equation (21) are able to track $r(t)$ and $\dot{r}(t)$, respectively, i.e., $\lim_{t\to\infty}[r(t) - r_1(t)] = 0$, $\lim_{t\to\infty}\left[\dot{r}(t) - r_2(t)\right] = 0$. For the parameter $\delta = 25{,}000$, the initial condition is set as $r_1(0) = 0$, $r_2(0) = 0$. In this algorithm, since the second order differential signal of the leg length signal is needed, two tracking differentiators are used serially to achieve the goal.

3.2. Controller Design of the Stewart Platform

As shown in Figure 6, $\boldsymbol{X}_c$ is the measured position (generalized position including translation and rotation) of the feed cabin, $\ddot{\widetilde{\boldsymbol{X}}}_c$ is the estimated acceleration of the feed cabin, and $\boldsymbol{X}_d, \dot{\boldsymbol{X}}_d, \ddot{\boldsymbol{X}}_d$ are the desired position, velocity and acceleration of the feed cabin, respectively. The parameters mentioned above are all described in inertial coordinate. Concerning the globally feedback linearized Stewart platform, the PID control law is designed as

$$\boldsymbol{F\prime} = \ddot{\boldsymbol{X}}_d - \ddot{\widetilde{\boldsymbol{X}}}_c + \boldsymbol{K}_p(\boldsymbol{X}_d - \boldsymbol{X}) + \boldsymbol{K}_d(\dot{\boldsymbol{X}}_d - \dot{\boldsymbol{X}}) + \boldsymbol{K}_i\int(\boldsymbol{X}_d - \mathbf{X})dt, \tag{24}$$

where $\boldsymbol{K}_p, \boldsymbol{K}_i, \boldsymbol{K}_d$ are diagonal controller gain matrices, each element of which is determined according to the control performance [28]. Noticing that these equations are described in the coordinate of the feed cabin, i.e., the acceleration is a relative value respect to the feed cabin, one can derive

$$\boldsymbol{F\prime} = \ddot{\boldsymbol{X}}_d - \ddot{\widetilde{\boldsymbol{X}}}_c + \boldsymbol{K}_p(\boldsymbol{X}_d - \boldsymbol{X}) + \boldsymbol{K}_d(\dot{\boldsymbol{X}}_d - \dot{\boldsymbol{X}}) + \boldsymbol{K}_i\int(\boldsymbol{X}_d - \mathbf{X})dt = \ddot{\boldsymbol{X}} - \ddot{\widetilde{\boldsymbol{X}}}_c. \tag{25}$$

Additionally, the incomplete linearization error stemmed from the unmodeled dynamics and parameters perturbation, together with the driving error of the electric cylinder, are considered as external disturbances [18,25]. By defining $\widetilde{\mathbf{E}} = \boldsymbol{X}_d - \mathbf{X}$, one can obtain,

$$\ddot{\widetilde{\boldsymbol{E}}} + \boldsymbol{K}_v\dot{\widetilde{\boldsymbol{E}}} + \boldsymbol{K}_p\widetilde{\boldsymbol{E}} + \boldsymbol{K}_i\int\widetilde{\mathbf{E}}dt = \boldsymbol{f}_{dist}. \tag{26}$$

It is assumed that the disturbance term $\boldsymbol{f}_{dist}$ is boundary, i.e., there exists a constant vector $\mathbf{a}$ satisfying

$$\max_t\left[\mathbf{f}_{dist}(t)\right]_i < a_i,\ i = 1, 2, \ldots, 6. \tag{27}$$

Then, from the linear control theory, one can design a controller so that the closed loop system is globally boundary input and boundary output stable [19,28]. Moreover, the condition of $t < 0$ leads to $\widetilde{E}_i(t) = 0$, and then, for $t > 0$, differentiation in both ends of Equation (26) with respect to time yields

$$\dddot{\widetilde{\mathbf{E}}} + \boldsymbol{K}_v\ddot{\widetilde{\mathbf{E}}} + \boldsymbol{K}_p\dot{\widetilde{\mathbf{E}}} + \boldsymbol{K}_i\widetilde{\mathbf{E}} = \dot{\mathbf{f}}_{dist} \tag{28}$$

From Equation (28), one can infer that for constant disturbance f_{dist}, the static error of the system $\widetilde{\mathbf{E}} = 0$ holds. In the simulation, the disturbance f_{dist} was set as zero-mean white noise signal with amplitude of 0.2 by trial and error [29]. The reason why the white noise is employed here lies in the complex internal and external perturbations of the system being difficult to describe; therefore, they are approximated by the white noise signal. As for the diagonal controller gain matrices $\boldsymbol{K}_p, \boldsymbol{K}_i, \boldsymbol{K}_d$, they were determined by analytical deduction with the pole placement method. The objective for designing the controller with pole placement method is the system damp ratio approaching 0.8, so that the system lies in the range of underdamped systems, displaying balanced settling time and overshoot.

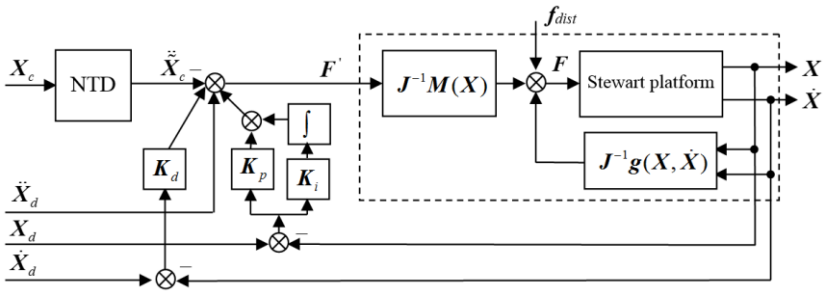

Figure 6. Controller of the cable-driven parallel manipulator (CDPM) based Stewart platform.

4. Experimental Apparatus

A FAST 50 m feed supporting and tracking system model shown in Figure 7 was constructed according to a 1/10 proportion of its prototype in Xidian University. It is expected to verify the mechatronic model and software and validate the complex control and measurement strategy. The height and radius of the distribution circle of the cable towers were designed according to the geometrical similarity with the ratio of 1/10. The movement specification of feed cabin in the FAST prototype is designed to reject the earth rotation when tracking a radio star. Therefore, the tracking velocity of feed cabin in the FAST 50 m model is also designed based on the geometrical similarity. By computation, this value is 3.5 mm/s.

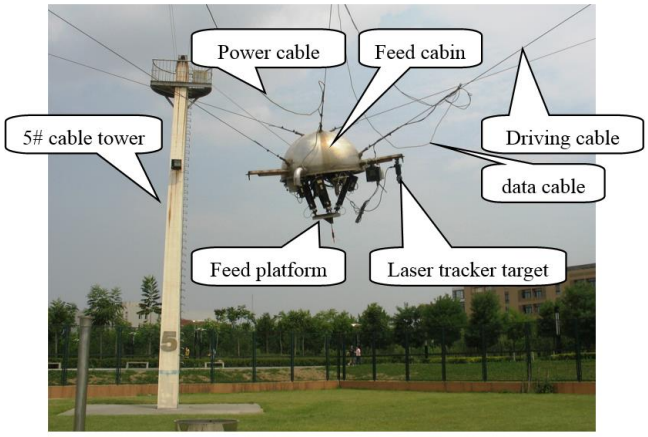

Figure 7. Field photo of the CDPM based Stewart platform.

The CDPM for coarse tuning is driven by six large span steel cable servo systems, with the semi-spherical feed cabin as the end-effector. In each of the six servo systems, there are a servo motor, a reducer, a wrench and two pulleys. The six cable towers have the same height of 21 m. The multi-stranded steel cable has a radius of 0.521 cm and a linear density of 0.14 kg/m. The feed cabin has a diameter of 1.0 m and a mass of 120.0 kg. Its center of gravity lies at the point 4.9 cm vertically from the center of the bottom.

The CDPM based Stewart platform employs THOMSON TN-series TN-BK23-10-5A-10 electric cylinders (Radford, VA, USA) with an incremental encoder (8192 P/5 mm). The electric cylinder has a stroke length of 254 mm and basic length of 146.1 mm. The main parameters are: maximum velocity 305 mm/s, maximum acceleration 7.7 m/s^2, maximum thrust 2670 N, total mass 5.5 kg, and repeatability $\pm$0.013 mm. The six drive units for the electric cylinders are connected one by one with RJ-45 cable, and then connected to the MEI network motion controller, which is inserted into the PCI (Peripheral Component Interconnect) socket of the micro tuning computer. The MEI XMP-SynqNet-PCI motion controller (Radford, VA, USA) is used here so that up to a 100 m remote control of the Stewart platform can be realized. The parameters of the motion controller are: DSP Analog Devices SHARC 32-bit floating point (Norwood, MA, USA), speed 40 MHz, update rate user programmable, and velocity, acceleration, jerk 32-bit floating point. The electric cylinder is running the torque mode under the MEI motion controller. The Stewart platform has a gross mass of 37.3 kg. The initial height of the feed platform, i.e., the center of the task space is -630 mm in the cabin frame.

There are four EVOC industrial computers with Pentium 4–2.4 GHz in total in the field model. The computers are connected to a local area network to communicate mutually and achieve the measuring and control goals. The task distribution of the four computers is as follows. The measuring computer deals with the real-time measuring data and sends them to the main control computer. The main control computer generates the motion trajectory of the macro-micro parallel manipulator system, and then sends the trajectory data to the macro tuning computer. The macro tuning computer conducts the kinetostatic computation and feedback control of the macro parallel manipulator with the pulse distribution card. The micro tuning computer carries out the decoupled position and orientation prediction, feedback control and kinematic computation of the Stewart platform, and then sends the control values of the six linear actuators to the MEI motion controller. In addition, each computer has a graphical user interface, which is used to display the status of the measuring and control processes and to input all kinds of commands and parameters.

5. Experiments and Discussion

The first experiment is related to the sinusoidal disturbance rejection of the CDPM based Stewart platform. This cable suspended system has better stiffness in Z (vertical direction) while weak stiffness in X and Y directions. In this case, the disturbance induced motion in X or Y directions attracted more attention. Therefore, the experiment of trajectory following in X, Y and Z directions were all conducted. However, for abbreviation, the paper only supplies the experimental result in the X direction. Similar conclusions can be drawn in these two horizontal directions. The air temperature was 18° C, and the maximum wind speed was 3.2 m/s. Since there is not a strong enough wind resulting in a large amplitude deviation of the feed cabin, the equivalent method of intentionally moving the cabin is proposed here. The feed cabin is controlled to move a sinusoidal displacement only in X with amplitude of 40 mm and a period of 14 s. The amplitude and period values came from the simulation of the FAST under permissive wind load with finite element method and were scaled down to the 1/10 model. The control goal is that the feed platform keeps still on a fixed point in the Cartesian coordinate system. Their trajectories are plotted in Figure 8. To observe the control performance in more detail, Figures 9–11 shows the positioning errors in X, Y and Z, respectively.

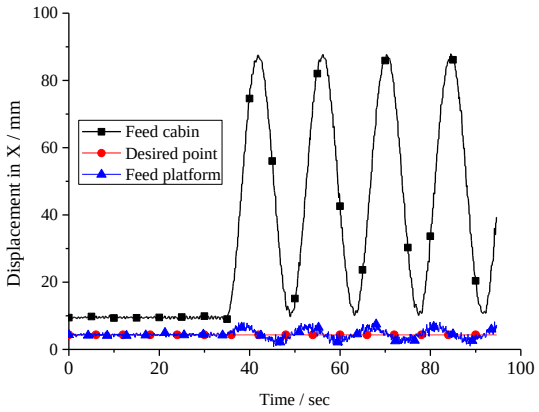

Figure 8. X Displacement of the feed cabin and platform.

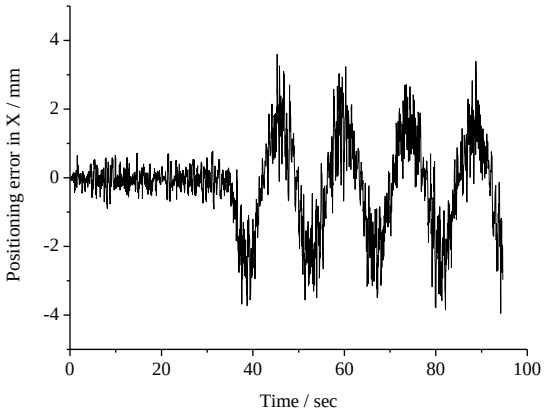

Figure 9. Positioning error of feed platform in *X*.

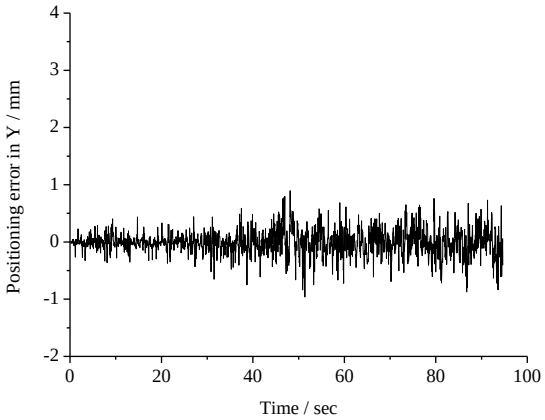

Figure 10. Positioning error of feed platform in *Y*.

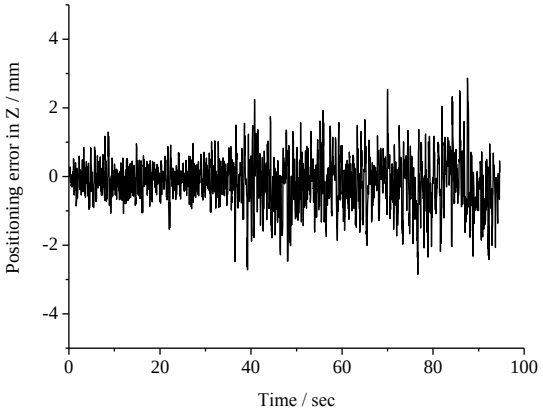

Figure 11. Positioning error of feed platform in *Z*.

From Figures 9–11, one can infer that the positioning error has a maximum of 4 mm. The result is able to meet the requirement of astronomy observation [1,3,6]. Moreover, the envelope of the error curve shows a similarity to the disturbance of the feed cabin. From the beginning to the 35th s, the feed cabin is commanded to remain static, but, as a result of the wind load and measurement noise, it vibrates in a tiny amplitude of less than 1 mm. In order to overcome the disturbance, the Stewart platform also moves with a tiny amplitude of less than 1mm as shown in Figure 9. The displacement of feed platform should be zero in both *Y* and *Z*; however, for a similar reason, the platform has positioning errors less than 2 mm in these two directions. The experiment verifies the effectiveness of the globally feedback linearization control of the CDPM based Stewart platform in local domain. By referring to the control performance with traditional kinematics approach reported in [4], the newly proposed approach achieves better performance in terms of precision.

The second experiment deals with a large trajectory area following the CDPM based Stewart platform, in which the feed cabin is designed to track a complete circle with radius of 0.5 m and height of 9.0 m. The control goal is that the feed platform will be able to track its desired curve in Figure 12, though there exists considerable error for the cabin trajectory tracking. The desired linear velocity for the feed cabin and platform is set as 5 mm/s. As for the orientation of the feed cabin and platform, it is prescribed that their normal directions point to a fixed point on the *Z*-axis of the inertial coordinates.

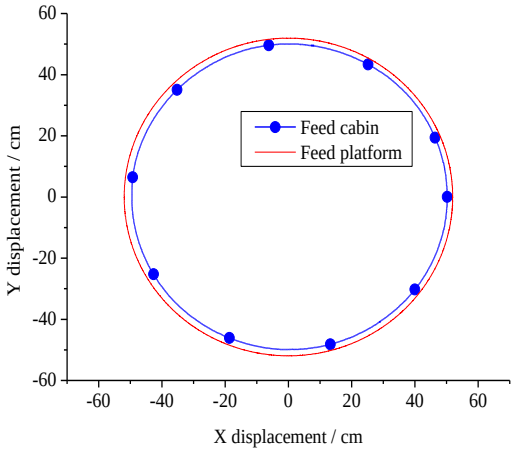

Figure 12. Trajectory projection of the feed cabin and platform in *XY*-plane.

Figures 13–15 show the positioning errors of the feed cabin and platform in *X*, *Y* and *Z*, respectively. The positioning error of the CDPM may come from the model perturbation, internal parameter variation and external wind load. One can notice this because of the flexibility of the six large

span cables with positioning errors in each direction of the feed cabin being over 1 cm, while the positioning error of the feed platform is limited to 2.5 mm. The CDPM based Stewart platform reduces the positioning error of the feed cabin in a translational direction by as much as 75%. In addition, the distribution of the platform errors is quite stationary. The control performance of this research satisfies the positioning specifications completely. It is noted that this positioning specification is obtained with a relatively low velocity of the feed cabin, which is determined by the law of similarity between the model and the prototype.

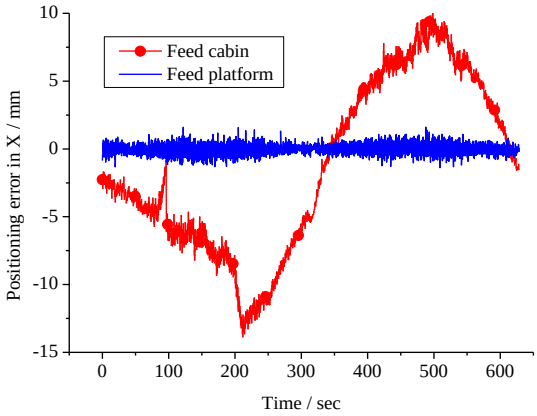

Figure 13. Positioning error in *X*.

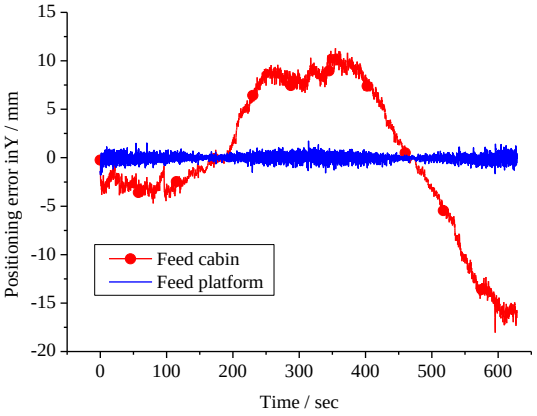

Figure 14. Positioning error in *Y*.

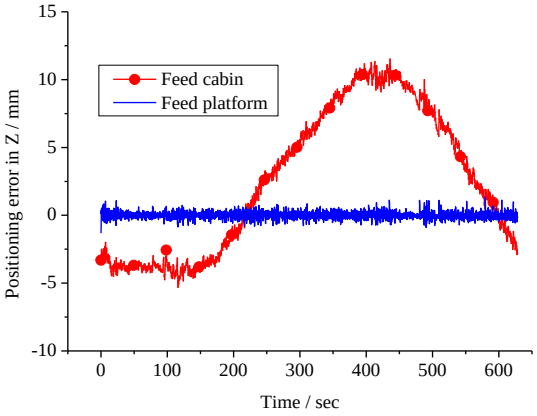

Figure 15. Positioning error in *Z*.

Figure 16 shows the pitch angle error of the feed cabin and platform. As an astronomical piece of equipment, the pitch angle precision of the platform will affect the observing result of the telescope, so enough attention should be paid to system design and controller tuning. The maximum pitch angle error of the cabin is up to 0.6°, while pitch angle error of the feed platform is restricted to 0.06°. Compared with error curves in the same level reported in [3], the position and pitch angle errors of the platform are displayed more uniformly. This experiment illustrates the effectiveness of the globally feedback linearization control of the CDPM based Stewart platform in a large domain.

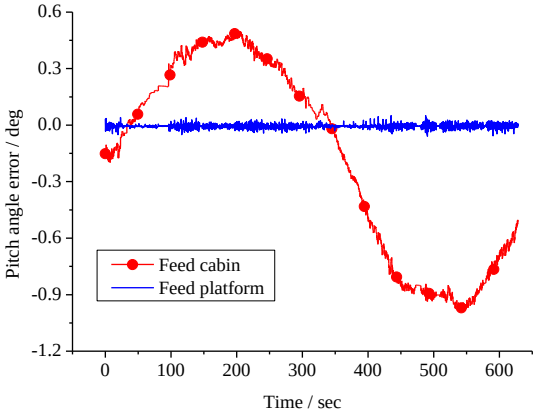

Figure 16. Pitch angle error.

6. Conclusions

The modeling, control and experiment of the CDPM based Stewart platform have been investigated in this paper. Some meaningful conclusions can be drawn as follows:

(1) The integrated dynamic model of the Stewart platform including the electric cylinder is established, and the global feedback linearization of the dynamic model is implemented based on the control law partitioning approach. Then, the approximated linear model is derived. This result lays a solid base for controller design in the operational space of the Stewart platform.

(2) A PID controller with base acceleration feedforward is designed in the operational space of the Stewart platform. In order to feed forward the dynamic information of the cabin into the control system of the Stewart platform, a novel nonlinear tracking differentiator is successfully employed to get the velocity and acceleration from the position information of the feed cabin.

(3) The experimental results of the FAST 50 m field model validate the effectiveness of the globally feedback linearization based PID control strategy, accompanied with the motion predication of the cabin; it manages to suppress the vibration of the feed cabin in local and large domains. The feed supporting, pointing and tracking system is able to meet the demands of positioning and orientating precision with the particular tracking velocity.

Future work related to this research includes the parameter optimization of the control scheme, mechatronic servo bandwidth [30] and control performance evaluation in the maximum workspace of the Stewart platform.

Acknowledgments: This work was supported by National Natural Science Foundation of China under Grant No. 51405362, the Natural Science Foundation of Shaanxi Province of China Grant No. 2016JQ5065, and the "111 project" under Grant No. B14042. The authors would also like to appreciate the editor, associate editors, and the reviewers for their valuable comments and suggestions.

Author Contributions: Xuechao Duan proposed the control scheme and wrote the paper; Jianwei Mi conceived the topic and developed the equations of dynamics; Ze Zhao developed the control codes and assisted with the experiment.

Conflicts of Interest: The authors declare no conflict of interest.

References

1. Nan, R. Five hundred meter aperture spherical radio telescope (FAST). *Sci. Chin. G* **2006**, *49*, 129–148. [CrossRef]
2. Shao, Z.; Tang, X.; Wang, L.; Chen, X. Dynamic modeling and wind vibration control of the feed support system in FAST. *Nonlinear Dyn.* **2012**, *67*, 965–985. [CrossRef]
3. Duan, X.; Qiu, Y.; Mi, J.; Zhao, Z. Motion prediction and supervisory control of the macro-micro parallel manipulator system. *Robotica* **2011**, *29*, 1005–1015. [CrossRef]
4. Duan, X.; Qiu, Y.; Bao, H.; Du, J. Real-time motion planning based vibration control of a macro-micro parallel manipulator system for super antenna. *J. Vibroeng.* **2014**, *16*, 694–703.
5. Du, J.; Bao, H.; Duan, X.; Cui, C. Jacobian analysis of a long-span cable-driven manipulator and its application to forward solution. *Mech. Mach. Theory* **2010**, *45*, 1227–1238. [CrossRef]
6. Qiu, Y.; Duan, B.; Wei, Q. Elimination of force singularity of the cable and cabin structure for the next generation large radio telescope. *Mechatronics* **2002**, *12*, 905–918. [CrossRef]
7. Stewart, D. A platform with six degrees of freedom. *Proc. Inst. Mech. Eng.* **1965**, *180*, 371–386. [CrossRef]
8. Merlet, J.P. *Parallel Robots*; Kluwer Academic Publisher: Dordrecht, The Netherlands, 2000.
9. Huang, Z.; Kong, L.; Fang, Y. *Mechanism Theory and Control of Parallel Robot*; Machine Industry Press: Beijing, China, 1997.
10. Dasgupta, B.; Mruthyunjaya, T.S. The Stewart platform manipulator: A review. *Mech. Mach. Theory* **2000**, *180*, 15–40. [CrossRef]
11. Ting, Y.; Chen, Y.; Jar, H.C. Modeling and control for a Gough-Stewart platform CNC machine. *J. Rob. Syst.* **2004**, *21*, 609–623. [CrossRef]
12. Lee, S.H.; Song, J.B.; Choi, W.C.; Hong, D. Position control of a Stewart platform using inverse dynamics control with approximate dynamics. *Mechatronics* **2003**, *13*, 605–619. [CrossRef]
13. Kim, D.; Kang, J.; Lee, K. Robust tracking control design for a 6 DOF parallel manipulator. *J. Rob. Syst.* **2000**, *17*, 527–547. [CrossRef]
14. Ding, B.; Cazzolato, B.S.; Stanley, R.M.; Grainger, S.; Costi, J.J. Stiffness analysis and control of a Stewart platform-based manipulator with decoupled sensor-actuator locations for ultrahigh accuracy positioning under large external loads. *J. Dyn. Syst. Meas. Contr.* **2014**, *136*, 061008. [CrossRef]
15. Chen, S.; Fu, L. Output feedback sliding mode control for a Stewart platform with a nonlinear observer-based forward kinematics solution. *IEEE Trans. Control Syst. Technol.* **2013**, *21*, 176–185. [CrossRef]
16. Zhang, H.; Wang, Q.; Wang, J. Interpolation for active vibration control of a Stewart platform. *J. Tsinghua Univ.* **2002**, *42*, 1473–1476.
17. Cheng, Y.; Ren, G.; Dai, S. Dynamic control simulation of Stewart platform with flexible suspension. *J. Tsinghua Univ.* **2003**, *43*, 1519–1522.
18. Zhou, Q.; Qi, L.; Zhang, H.; Duan, G. Experiments on active large-amplitude vibration control of a coupled Stewart platform. *Chin. Mech. Eng.* **2005**, *16*, 1599–1602.
19. Craig, J.J. *Introduction to Robotics: Mechanics and Control*, 3rd ed.; Prentice Hall: Upper Saddle River, NJ, USA, 2004.
20. Duan, X.; Qiu, Y.; Duan, Q.; Du, J. Calibration and Motion Control of a Cable-Driven Parallel Manipulator Based Triple-Level Spatial Positioner. *Adv. Mech. Eng.* **2014**, *2014*, 368018. [CrossRef]
21. Ogata, K. *Modern Control Engineering*, 5th ed.; Prentice Hall: Upper Saddle River, NJ, USA, 2009.
22. Angeles, J. *Fundamentals of Robotic Mechanical Systems: Theory, Methods, and Algorithms*, 4th ed.; Springer: New York, NY, USA, 2014.
23. Su, Y.; Duan, B.; Zheng, C. Nonlinear PID control of a six-DOF parallel manipulator. *IET Control Theory Appl.* **2004**, *151*, 95–102. [CrossRef]
24. Dasgupta, B.; Mruthyunjaya, T.S. Newton-Euler formulation for the inverse dynamics of the Stewart platform manipulator. *Mech. Mach. Theory* **1998**, *33*, 1135–1152. [CrossRef]
25. Fu, S.; Yao, Y.; Wu, Y. Comments on "A Newton-Euler formulation for the inverse dynamics of the Stewart platform manipulator" by B. Dasgupta and T.S. Mruthyunjaya [Mech. Mach. Theory 33 (1998) 1135–1152]. *Mech. Mach. Theory* **2007**, *42*, 1668–1671. [CrossRef]
26. Han, J. *Active Disturbance Rejection Control Technique—the Technique for Estimating and Compensating the Uncertainties*; National Defense Industry Press: Beijing, China, 2008.

27. Han, J. Active disturbances rejection control technique. *Front. Sci.* **2007**, *1*, 24–31.
28. Franklin, G.F.; Powell, J.D.; Emami-Naeini, A. *Feedback Control of Dynamic Systems*, 4th ed.; Prentice Hall: New York, NY, USA, 2002.
29. Liu, J.K. *Control System Design and MATLAB Simulation*; Tsinghua University Press: Beijing, China, 2008.
30. Duan, X.; Qiu, Y.; Mi, J.; Bao, H. On the mechatronic servo bandwidth of a Stewart platform for active vibration isolating in a super antenna. *Rob. Comput. Integr. Manuf.* **2016**, *40*, 66–77. [CrossRef]